ACS APPLIED MATERIALS & INTERFACES

Letter

www.acsami.org

Surface-Dependent Self-Assembly of Conducting Polypyrrole Nanotube Arrays in Template-Free Electrochemical Polymerization

Jingwen Liao,[†,‡] Shuilin Wu,[†,§,⊥] Zhaoyi Yin,[∥] Shishu Huang,[#] Chengyun Ning,*[,‡] Guoxin Tan,[△] and Paul K. Chu*[,⊥]

[‡]School of Materials Science and Engineering, South China University of Technology, Guangzhou 510641, China

[§] Hubei Collaborative Innovation Center for Advanced Organic Chemical Materials, Ministry-of-Education Key Laboratory for the Green Preparation and Application of Functional Materials, Faculty of Materials Science & Engineering, Hubei University, Wuhan 430062, China

[⊥]Department of Physics and Materials Science, City University of Hong Kong, Tat Chee Avenue, Kowloon, Hong Kong, China

[∥]School of Materials Science and Technology, Kunming University of Science and Technology, Kunming 650093, China

[#]State Key Laboratory of Oral Diseases, West China Hospital of Stomatology, Sichuan University, Chengdu 610041, China

[△]Institute of Chemical Engineering and Light Industry, Guangdong University of Technology, Guangzhou 510006, China

Supporting Information

ABSTRACT: One-dimensional conducting polymer nanostructure arrays could provide short ion transport paths, thus delivering superior chemical/physical performance and having large potential as intelligent switching materials. In this work, in situ electrochemical atomic force microscopy is employed to monitor the self-assembly of conducting polypyrrole nanotube arrays in template-free electrochemical polymerization. The specific spreading behavior of pyrrole micelles on the conductive substrate is important to large-area self-assembly of conducting polypyrrole nanotube arrays and the insight into self-assembly of conducting polypyrrole nanotube arrays is discussed. Moreover, compared with unoriented nanostructured polypyrrole, the conducting polypyrrole nanotube arrays possess enhanced electrical and electrochemical performances.

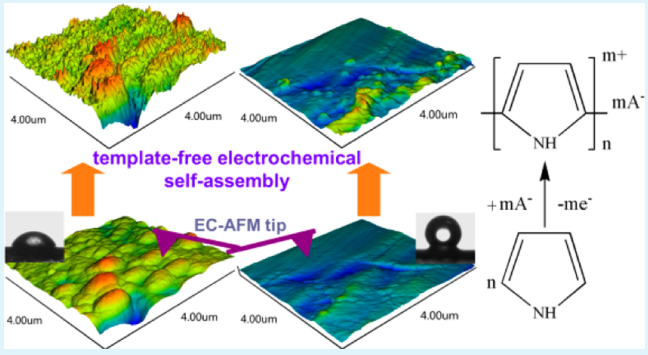

KEYWORDS: *conducting polymers, self-assembly, electrochemical polymerization, EC-AFM, nanotubes*

Nanostructured materials are used in a myriad of biological, electrical, and optical devices.[1−3] One-dimensional (1D) nanostructured arrays possess superior chemical/physical properties and have been applied in several fields, such as chemical sensors,[4] microelectronics,[5] and supercapacitors,[6] etc. Among multiple technologies for nanofabrication of 1D nanostructured arrays, template-based approaches are quite common and flexible. However, removing of the templates, such as anodic aluminum oxide and track-etched polycarbonate, may be troublesome, and leads to aggregation and damage of the nanostructures.[7,8] Therefore, both scientific and technological interests have been focused on "template-free" preparation of 1D nanostructured arrays by the vapor−liquid−solid approach,[7,8] gas solid reaction method,[9] solution-solid reaction,[10] and in situ fabrication.[11,12] The template-free strategies are mainly devoted to inorganic (carbon, metals, semiconductors and oxides) 1D nanostructured arrays. Nonetheless, less effort has been devoted to organic and polymeric ones.[6,13]

Conducting polymers (CPs), one type of functional polymers with electroactivity,[14,15] exhibit excellent biological tissue compatibility, redox reversibility, and environmental stability.[16−18] 1D CP nanostructure arrays, such as CP nanowire arrays and CP nanotube arrays, have aroused much interest among scientists due to the short transport path for ions and large surface area, thus boding well for potential applications in chemical/biological sensing,[4] drug delivery, energy storage,[6] and intelligent switching materials.[19,20] The template-free electrochemical technique which is associated with the self-assembly using basic building nanoblocks, is applicable for 1D CP nanostructured arrays.[4,6,21,22] The self-assembly efficacy depends on the electrochemical conditions and specific surfaces of the substrates, for example, conductive substrate as the working electrode. Galvanostatic fabrication of large-area CP nanowire arrays has been demonstrated on conductive substrates coated with polyaniline and Au nanoislands.[4,6] These layers have been proved pseudonucleation sites

Received: March 23, 2014
Accepted: July 9, 2014
Published: July 9, 2014

for the CPs, thus allowing the fabrication of 1D CP nanostructure arrays over a large area. In spite of experimental success, the mechanism is still not well known.

In the attempt to fabricate nanostructured CPs using a template-free electrochemical approach, we find it hard to harvest a large area on the surface of some conductive substrate (e.g., titanium (Ti)), which may result from the incapability of substrate to form sufficient active nucleation sites. As such, several modification layers are introduced on Ti substrate to tune the capability for forming active nucleation sites. In this work, the in situ electrochemical atomic force microscopy (EC-AFM) is employed to track the self-assembly process of conducting polypyrrole (PPy) nanotube arrays (CPNAs) during template-free electrochemical polymerization. The surface characteristic of conductive substrate, that is, spreading behaviors of Py micelles on Ti and Ti coated with a thin PPy film (termed as prenucleation film, PNF) doped with Cl^- (designated as PNF/Cl−Ti) are investigated for the self-assembly of CPNAs. In addition, the self-assembly on Ti coated with PNF doped with β-naphthalenesulfonic acid (NSA) (labeled as PNF/NSA-Ti) in various redox states as well as on Ti coated with a layer of gold (Au−Ti) are also determined. As detailed in the experimental details in the Supporting Information, the PNF/Cl−Ti and Ti as the working electrodes are placed on a Petri dish (Figure 1a) for in situ EC-AFM. Before the fabrication of the nanostructured conducting PPy on the working electrode, the spreading behavior (inset of Figure 1b) of the Py microdroplet (1 μL) on PNF/Cl−Ti is clearly different from that on Ti. The surface contact angles are 64.3 ± 2.5° on PNF/Cl−Ti and 133.8 ± 3.8° on Ti. The in situ EC-AFM height images of the nanostructured conducting PPy on PNF/Cl−Ti and Ti obtained from different points in time are depicted in Figure 1b. On PNF/Cl−Ti (Figure 1b1), surface fluctuations are obvious in the three-dimensional (3D) AFM image (0 s) compared to two-dimensional (2D) field-emission scanning electron microscopy (FE-SEM, ZEISS Ultra 55, Germany) image (data not shown here). After 5 s of template-free electrochemical polymerization, protuberant nanoparticles are faintly visible on PNF/Cl−Ti and clearly visible at 45 s. As proceeding further, the protuberant nanoparticles become into nanoneedled structures at 2 min and into 1D nanostructure arrays at 5 min, accompanying with the disappearance of surface fluctuations. The FE-SEM and transmission electron microscopy (TEM, JEOL JEM-2100, Japan) images (Figure 1c1) reveal that hollow nanotubular structure with an inner diameter of about 30 nm and outer diameter of approximately 60 nm (top section) are vertical to the PNF/Cl−Ti over a large area. On the Ti substrate, the EC-AFM images (Figure 1b2) disclose that the self-assembly process is very different from that on PNF/Cl−Ti. The surface of Ti (0 s) is smoother and as the process continues, only the changes in the surface roughness and color can be identified, implying an increase in height or thickness in a small area with time. Although no well-defined nanostructures can be observed by EC-AFM, it is believed that the rough area offers preferential sites for self-assembly of nanostructured conducting PPy, which is indeed confirmed by the FE-SEM image (Figure 1c2) showing disordered nanoclusters at a small density.

To elucidate the growth mechanism, besides PNF/Cl−Ti and Ti, PNF/NSA-Ti in various redox states and Au−Ti as conductive substrates are studied. As shown in Figure 2, the surface contact angles (spreading behavior of Py microdroplet in electrolyte) of PNF/NSA-Ti in original state (2a1), reduced

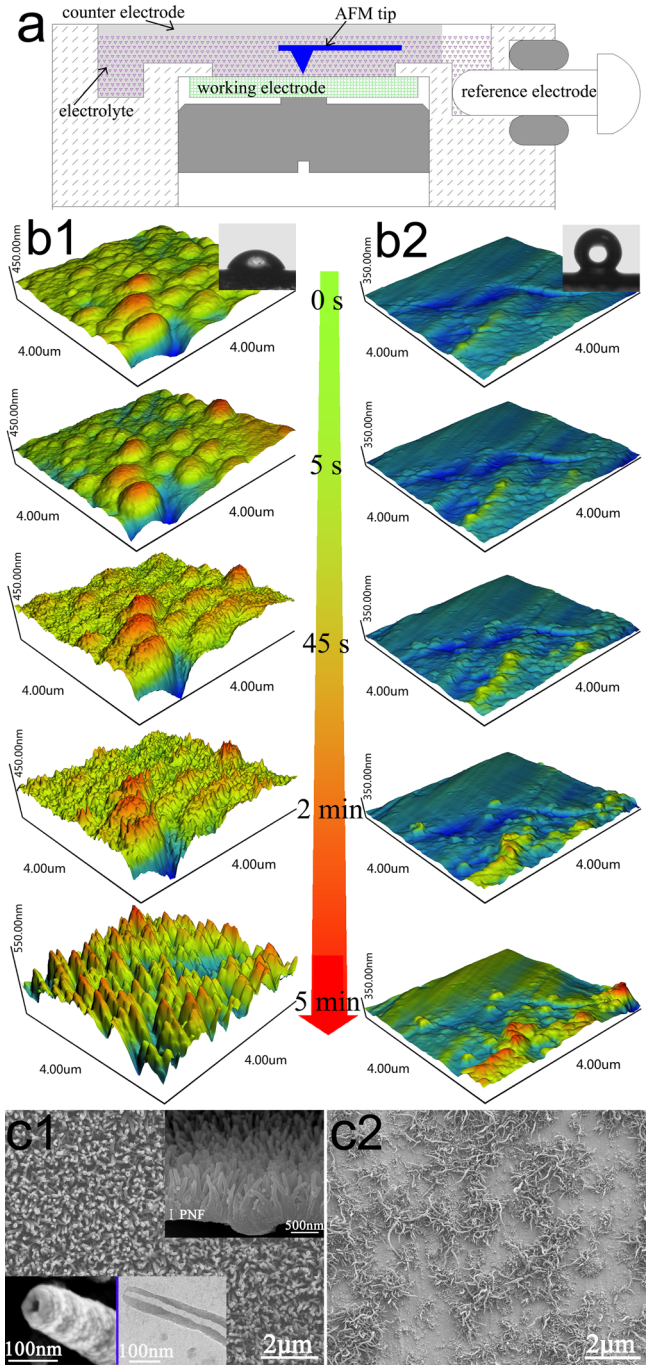

Figure 1. (a) Cross-section of Petri dish for EC-AFM. (b) Height images of self-assembly fabrication process (0 s, 5 s, 45 s, 2 min, 5 min) of nanostructured conducting PPy on PNF/Cl−Ti (1) and Ti (2) were recorded by in situ EC-AFM, insert: spread of Py droplet on PNF/Cl−Ti and Ti. (c) FE-SEM images of nanostructured conducting PPy fabricated (7 min) on PNF/Cl−Ti (1) and Ti (2); insets: cross-sectional view (SEM) and nanotubular structure (FE-SEM and TEM).

sate (2a2), and oxidized state (2a3) are 80.1 ± 2.7°, 16.9 ± 1.1°, and 141.1 ± 3.4°, respectively. The difference of spreading behavior is due to the changes of NSA strength on PNF/NSA-Ti surface with various redox states, which, as shown in Figure S2 in the Supporting Information, is verified by electron probe microanalyzer (EPMA, Shimadzu 1720, Japan) technique. Through self-assembly on PNF/NSA-Ti in original state, the

dx.doi.org/10.1021/am5017478 | ACS Appl. Mater. Interfaces 2014, 6, 10946−10951

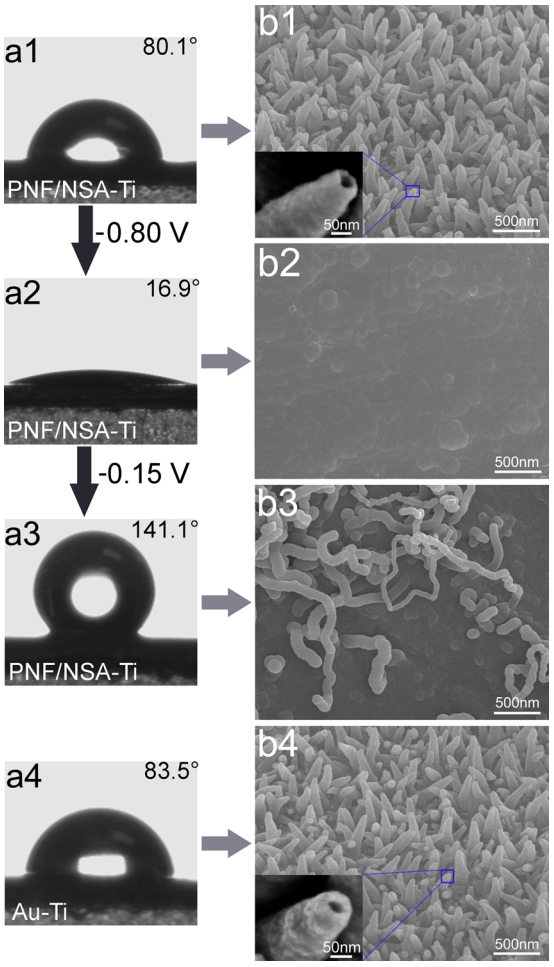

Figure 2. (a) Surface contact angle images of the Py microdroplet and (b) FE-SEM images of the nanostructured conducting PPy grown on PNF/NSA-Ti in original state (1), reduced state (2), oxidized state (3), and on Au−Ti (4). Insets in b1 and b4: higher magnification.

large-area aligned nanostructured conducting PPy with a hollow structure (inner diameter of about 30 nm) is formed, which can be found in Figure 2b1. An irregular film (Figure 2b2) showing vague nanoparticle grows on PNF/NSA-Ti in reduced state, whereas twisty nanowires (Figure 2b3) with a small density on PNF/NSA-Ti in oxidized state. Although the chemical composition of Au−Ti is different from PNF/NSA-Ti, Au−Ti shows a similar spreading behavior of Py microdroplet (83.5 ± 3.0°, Figure 2a4) and subsequently harvests the same CPNAs (Figure 2b4) as that on PNF/NSA-Ti in original state. It should herein be noted that various redox states of PNF/NSA-Ti must be returned to the same final state (i.e., oxidized state) once the electrochemical polymerization is triggered, and nevertheless the spreading behavior has already been achieved before the returning (i.e., spreading behaviors here are discussed before not after the electrochemical polymerization). Hence, the spreading behavior of the Py microdroplet on the conductive substrate plays an important role in large-area self-assembly of CPNAs, which is independent of surface chemical composition of conductive substrates.

The schematic describing an insight into self-assembly of CPNAs in template-free electrochemical polymerization is discussed in Figure 3. The Py micelles with a diameter of about 60 nm (Figure 3a*, measured by zetasizer nanoanalyzer (Malvern Nano-ZS, Britain)) are stabilized by NSA (i.e., Py-NSA micelles) and dispersed in phosphate buffer solution (PBS) as the electrolyte. It is noteworthy that the PBS renders the polymerization of Py a stable medium with constant pH, which is one of important factors for fabricating fine nanostructures. The electrode surface then attracts ("anchor" as metaphor) Py-NSA micelles due to the positive potential. Owing to Py-repellence (Figure 3b1) on the PNF-Ti surface (Ti and PNF/NSA-Ti in oxidized state), most of Py-NSA micelles are unable to be free from the anchors whereas Figure 3c1 and 3d1 show that all the Py-NSA micelles are free from the anchors and thereby supporting firm adhesion of micelles on the PNF-Ti surface (PNF/Cl−Ti, and PNF/NSA-Ti in the original state and reduced state). Only when the Py-NSA micelles spread on the electrode can the electrochemical polymerization of Py-NSA micelles be triggered.

Because the Py-NSA micelles hold their shape (poor spreading behavior), the Py-NSA micelles are prone to being free from the anchors, electrochemical polymerization of Py is triggered from the bottom of the Py-NSA micelles layer by layer, and subsequently the solid nanograins (Figure 3b2, b2*) appear on PNF-Ti. Because of the small density and being surrounded by micelles/anchors, the nanograins are in anisotropic space and the self-assembly of Py-NSA micelles on the nanograins is out of order (Figure 3b3), thus resulting in the formation of short crooked nanowires or long crooked nanograins (Figure 3b4). By subsequent self-assembly, grasslike twisty nanowires (Figure 3b5) with a small density are produced.

As shown in illustrations c2 and c3 in Figure 3, the Py-NSA micelles fully spread (good spreading behavior) on the PNF-Ti and are electropolymerized into nanohills which randomly guide self-assembly of the Py-NSA micelles. As a result, overlapping nanohills (Figure 3c4) are formed and evolved into an irregular film (Figure 3c5) that can be observed from Figure 2b2. The appropriate spreading behavior of Py-NSA micelles facilitates preferential electrochemical polymerization at the interface and bottom of the Py-NSA micelles. Then Py monomers in the micelles migrate to the reaction areas (interface and bottom). Naturally, nanocavities (Figure 3d2, d2*) are produced after the depletion of monomer in micelles whose sizes are smaller than that of Py-NSA micelles due to a volume shrinkage during the polymerization of Py-NSA micelles. Here, the isotropic two-dimensional platform created by the nanocavities with a high density, in conjunction with the edge effect affording higher electric field,[23] enables the Py-NSA micelles to orderly self-assembling (Figure 3d3) on the nanocavities, then forming short cylindrical nanotubes (Figure 3d4). As self-assembly proceeding further, large-area cylindrical CPNAs (Figure 3d5) are vertically grown on the PNF-Ti. The results suggest that the conductive substrate which is capable of producing the specific spreading behavior of Py-NSA micelles creates isotropic two-dimensional space, which is a precondition for adequate nucleation sites and subsequent large-area self-assembly of CPNAs. In addition, because the solubility of Py monomers is relatively low in this electrolyte and most of dissolved Py monomers are consumed in the polymerization on outer surface of CPNAs (conical shape in Figure 2b1 and 2b4), the amount of dissolved Py polymerizing on inner surface of CPNAs is negligible. As such, the nanotubular structure remains unchanged.

The electrical and electrochemical properties of diverse nanostructures of PPy obtained by various self-assembly modes but with the same deposition charge (0.9 mA/cm^2 for 5 min)

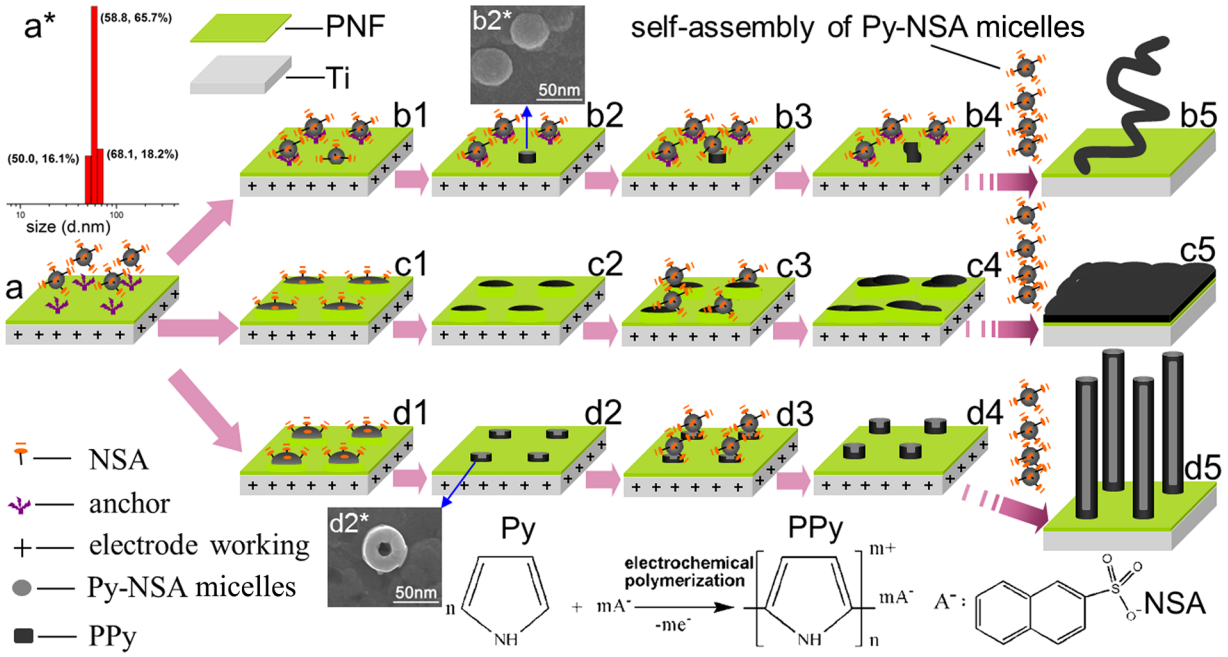

Figure 3. Schematic illustration of the fabrication process of the nanostructured conducting PPy via template-free electrochemical polymerization: (a) Py-NSA micelles with a diameter of about 60 nm (a*) dispersed in PBS, PNF-Ti (electrode surface) are apt to adsorb ("anchor" as metaphor here) Py-NSA micelles. (Letter +1) Py-NSA micelles free from anchors and spread on PNF-Ti depending on the spreading behavior on PNF-Ti. Free Py-NSA micelles undergo polymerization producing (b2, b2*) nanograins, (c2) nanohills, and (d2, d2*) nanocavities. Py-NSA micelles self-assemble on (b3) nanograins (disordered), (c3) nanohills (disordered), and (d3) nanocavities (ordered). (b4) Short crooked nanowires, (c4) overlapping nanohills, and (d4) short cylindrical nanotubes are obtained. Twisty nanowires with a (b5) small density, (c5) irregular film, and (d5) cylindrical nanotube arrays with a large density are fabricated on PNF-Ti by self-assembly.

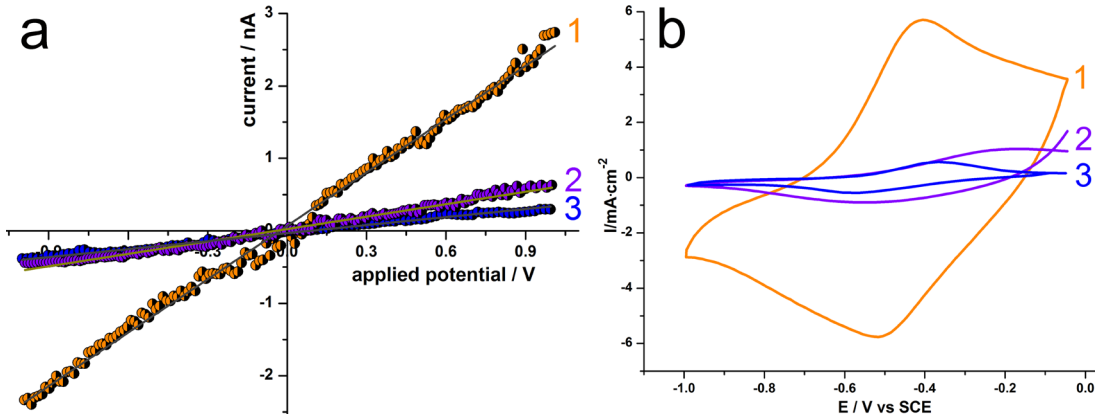

Figure 4. (a) CP-AFM $I-V$ measurements and (b) cyclic voltammograms of diverse nanostructures of PPy. (1) Nanotube arrays. (2) Twisty nanowires. (3) Irregular film.

are investigated by conductive-probe atomic force microscopy (CP-AFM, PtIr AFM tip) and cyclic voltammetry. As illustrated in Figure 4a, the three local $I-V$ plots show linear behaviors. The plots of CPNAs (Figure 4a1) and irregular film (Figure 4a3) exhibit a largest and smallest slope, respectively, indicating a highest conductivity (83.9 S cm^{-1}) of CPNAs and a lowest conductivity (11.3 S cm^{-1}) of irregular film. Regarding to electrochemical activity, as disclosed in Figure 4b, all cyclic voltammograms recorded in Py-free PBS (pH 6.8) containing 0.01 M NSA at a rate of 10 mV/s are characterized by reduction and oxidation peaks, showing good x axis symmetry thus demonstrating the electroactivity and good redox reversibility. Differently, the current values of redox peaks in Figure 4b1 (CPNAs) are both considerably larger than that in Figure 4b2 (twisty nanowires) and Figure 4b3 (irregular film). Therefore, compared with the unoriented nanostructured PPy, the1D CPNAs conferring enhanced electrical and electrochemical properties may be due to (a) the higher active surface area accessible to the electrolyte, (b) the shorter ion transport paths to electrolyte, and (c) smoother electron flow in oriented nanostructured matrix, which is desirable for high efficiency and sensitivity of numerous microelectronics devices.

In summary, the in situ EC-AFM discloses that the spreading behavior of Py micelles on conductive substrate, plays a crucial role in large-area self-assembly of the CPNAs. We accordingly propose an insight into the large-area self-assembly fabrication of CPNAs via template-free electrochemical polymerization. The conductive substrate allowing specific spreading behavior of the Py micelles with a surface contact angle between about 60° and 90° facilitates the fabrication of CPNAs by template-

dx.doi.org/10.1021/am5017478 | ACS Appl. Mater. Interfaces 2014, 6, 10946−10951

free self-assembly on a large area. It should be noted that, like most of studies on self-assembly of nanomaterials, there must not only be one factor (such as surface characteristic of conductive substrate) but also other factors (such as electrochemical approaches, etc, as seen in Figures S3 and S4 in the Supporting Information) that play necessary roles in fabrication of nanostructures. We herein focus on the effect of surface characteristic of conductive substrate on the self-assembly of CPNAs under the same other conditions. Moreover, compared with unoriented nanostructured PPy, the CPNAs possess enhanced electrical and electrochemical performances. This study can be extended to the fabrication of other CPs and 1D nanostructured arrays of electro-active materials of potential applications in biosensors, drug delivery systems, energy storage, and intelligent switching materials. Promisingly, CPNAs as electroactive 1D nanostructured arrays in conjunction with unique material properties provide an avenue for some sophisticated applications such as bioinspired ion channels/pumps,[24−27] etc.

■ ASSOCIATED CONTENT

Ⓢ Supporting Information

Fabrication methods of PNF/Cl and PNF/NSA in the various redox states, self-assembly fabrication of CPNAs monitored by in situ EC-AFM, self-assembly of CPNAs using Au−Ti and PNF/NSA with various redox states, and details of the electrochemical system. This material is available free of charge via the Internet at http://pubs.acs.org.

■ AUTHOR INFORMATION

Corresponding Authors

*E-mail: imcyning@scut.edu.cn.

*E-mail: paul.chu@cityu.edu.hk.

Author Contributions

[†]J.L. and S.W. contributed equally to the work and share cofirst authorship.

Notes

The authors declare no competing financial interest.

■ ACKNOWLEDGMENTS

This work was jointly supported by National Basic Research Program of China (Grant 2012CB619100), the National Natural Science Foundation of China (Grants 51372087, 51072057, 51101053, and 81271715), Hong Kong Research Grants Council (RGC) General Research Funds (GRF) 112212, and City University of Hong Kong Applied Research Grants (ARG, 9667066 and 9667069).

■ REFERENCES

(1) Zhang, W.; Yang, S. In Situ Fabrication of Inorganic Nanowire Arrays Grown from and Aligned on Metal Substrates. *Acc. Chem. Res.* **2009**, *42*, 1617−1627.

(2) Jiang, J.; Li, Y.; Liu, J.; Huang, X. Building One-Dimensional Oxide Nanostructure Arrays on Conductive Metal Substrates for Lithium-Ion Battery Anodes. *Nanoscale* **2011**, *3*, 45−58.

(3) Cui, Y.; Wei, Q.; Park, H.; Lieber, C. M. Nanowire Nanosensors for Highly Sensitive and Selective Detection of Biological and Chemical Species. *Science* **2001**, *293*, 1289−1292.

(4) Liu, J.; Lin, Y.; Liang, L.; Voigt, J. A.; Huber, D. L.; Tian, Z. R.; Coker, E.; Mckenzie, B.; Mcdermott, M. J. Templateless Assembly of Molecularly Aligned Conductive Polymer Nanowires: A14 New Approach for Oriented Nanostructures. *Chem.—Eur. J.* **2003**, *9*, 604−611.

(5) Hu, Z.; Tian, M.; Nysten, B.; Jonas, A. M. Regular Arrays of Highly Ordered Ferroelectric Polymer Nanostructures for Non-Volatile Low-Voltage Memories. *Nat. Mater.* **2008**, *8*, 62−67.

(6) Huang, J.; Wang, K.; Wei, Z. Conducting Polymer Nanowire Arrays with Enhanced Electrochemical Performance. *J. Mater. Chem.* **2010**, *20*, 1117−1121.

(7) Wang, X.; Song, J.; Li, P.; Ryou, J. H.; Dupuis, R. D.; Summers, C. J.; Wang, Z. L. Growth of Uniformly Aligned ZnO Nanowire Heterojunction Arrays on GaN, AlN, and Al0. 5Ga0. 5N Substrates. *J. Am. Chem. Soc.* **2005**, *127*, 7920−7923.

(8) He, R.; Gao, D.; Fan, R.; Hochbaum, A. I.; Carraro, C.; Maboudian, R.; Yang, P. Si Nanowire Bridges in Microtrenches: Integration of Growth into Device Fabrication. *Adv. Mater.* **2005**, *17*, 2098−2102.

(9) Ji, H. X.; Hu, J. S.; Guo, Y. G.; Song, W. G.; Wan, L. J. Ion-Transfer-Based Growth: A Mechanism for CuTCNQ Nanowire Formation. *Adv. Mater.* **2008**, *20*, 4879−4882.

(10) Yang, J.; Qiu, Y.; Yang, S. Studies of Electrochemical Synthesis of Ultrathin ZnO Nanorod/Nanobelt Arrays on Zn Substrates in Alkaline Solutions of Amine-Alcohol Mixtures. *Cryst. Growth Des.* **2007**, *7*, 2562−2567.

(11) Huang, S.; Ning, C.; Peng, W.; Dong, H. Anodic Formation of Ti Nanorods with Periodic Length. *Electrochem. Commun.* **2012**, *17*, 14−17.

(12) Huang, S.; Peng, W.; Ning, C.; Hu, Q.; Dong, H. Nanostructure Transition on Anodic Titanium: Structure Control via a Competition Strategy between Electrochemical Oxidation and Chemical Etching. *J. Phys. Chem. C* **2012**, *116*, 22359−22364.

(13) Li, M.; Wei, Z.; Jiang, L. Polypyrrole Nanofiber Arrays Synthesized by a Biphasic Electrochemical Strategy. *J. Mater. Chem.* **2008**, *18*, 2276−2280.

(14) Liao, J.; Pan, H.; Ning, C.; Tan, G.; Zhou, Z.; Chen, J.; Huang, S. Taurine-Induced Fabrication of Nano-Architectured Conducting Polypyrrole on Biomedical Titanium. *Macromol. Rapid Commun.* **2014**, *35*, 574−578.

(15) Chiang, C.; Fincher, C., Jr.; Park, Y.; Heeger, A.; Shirakawa, H.; Louis, E.; Gau, S.; MacDiarmid, A. G. Electrical Conductivity in Doped Polyacetylene. *Phys. Rev. Lett.* **1977**, *39*, 1098−1101.

(16) Chen, M.; Fang, X.; Tang, S.; Zheng, N. Polypyrrole Nanoparticles for High-Performance In Vivo Near-Infrared Photothermal Cancer Therapy. *Chem. Commun.* **2012**, *48*, 8934−8936.

(17) Guimard, N. K.; Gomez, N.; Schmidt, C. E. Conducting Polymers in Biomedical Engineering. *Prog. Polym. Sci.* **2007**, *32*, 876−921.

(18) Darmanin, T.; Bellanger, H.; Guittard, F.; Lisboa, P.; Zurn, M.; Colpo, P.; Gilliland, D.; Rossi, F. Structured Biotinylated Poly (3, 4-ethylenedioxypyrrole) Electrodes for Biochemical Applications. *RSC Adv.* **2012**, *2*, 1033−1039.

(19) Liao, J.; Ning, C.; Yin, Z.; Tan, G.; Huang, S.; Zhou, Z.; Chen, J.; Pan, H. Nanostructured Conducting Polymers as Intelligent Implant Surface: Fabricated on Biomedical Titanium with a Potential-Induced Reversible Switch in Wettability. *ChemPhysChem* **2013**, *14*, 3891−3894.

(20) Liao, J.; Huang, S.; Ning, C.; Tan, G.; Pan, H.; Zhang, Y. Potential-Induced Reversible Switch in Tubular Structure of Conducting Polypyrrole Nanotube Arrays. *RSC Adv.* **2013**, *3*, 14946−14949.

(21) Liang, L.; Liu, J.; Windisch, C. F., Jr.; Exarhos, G. J.; Lin, Y. Direct Assembly of Large Arrays of Oriented Conducting Polymer Nanowires. *Angew. Chem., Int. Ed.* **2002**, *41*, 3665−3668.

(22) Huang, J.; Quan, B.; Liu, M.; Wei, Z.; Jiang, L. Conducting Polypyrrole Conical Nanocontainers: Formation Mechanism and Voltage Switchable Property. *Macromol. Rapid Commun.* **2008**, *29*, 1335−1340.

(23) Akahane, Y.; Asano, T.; Song, B. S.; Noda, S. High-Q Photonic Nanocavity in a Two-Dimensional Photonic Crystal. *Nature* **2003**, *425*, 944−947.

(24) Zhang, Q.; Liu, Z.; Hou, X.; Fan, X.; Zhai, J.; Jiang, L. Light-Regulated Ion Transport through Artificial Ion Channels Based on TiO_2 Nanotubular Arrays. *Chem. Commun.* **2012**, *48*, 5901−5903.
(25) Zhang, H.; Hou, X.; Zeng, L.; Yang, F.; Li, L.; Yan, D.; Tian, Y.; Jiang, L. Bioinspired Artificial Single Ion Pump. *J. Am. Chem. Soc.* **2013**, *135*, 16102−16110.
(26) Tian, Y.; Wen, L.; Hou, X.; Hou, G.; Jiang, L. Bioinspired Ion-Transport Properties of Solid-State Single Nanochannels and Their Applications in Sensing. *ChemPhysChem* **2012**, *13*, 2455−2470.
(27) Kong, Y.; Fan, X.; Zhang, M.; Hou, X.; Liu, Z.; Zhai, J.; Jiang, L. Nanofluidic Diode Based on Branched Alumina Nanochannels with Tunable Ionic Rectification. *ACS Appl. Mater. Interfaces* **2013**, *5*, 7931−7936.